ACS EARTH AND SPACE CHEMISTRY

http://pubs.acs.org/journal/aesccq
Article

Solar Wind Irradiation of Methane and Methane−Water Ices: A Molecular Dynamics Approach

Alessandra Ricca* and Justin B. Haskins

Cite This: ACS Earth Space Chem. 2024, 8, 2509−2521
Read Online
ACCESS | Metrics & More | Article Recommendations

ABSTRACT: Molecular dynamics simulations were performed to characterize reaction products, resulting from solar wind irradiation, namely, H^+, of methane and methane−water ices. In our approach, we used seven 0.829 keV H^+ (total energy of 5.8 keV), with a velocity of 400 km/s, to hit the icy surface simultaneously, and we repeated this process multiple times to simulate continuous irradiation while quenching the ice to 15 K after each irradiation to prevent excessive heating and sublimation. Our simulations produced complex organic molecules previously obtained in laboratory experiments. For methane ice, molecules containing two carbons were predominant, with ethane and ethyl radicals being the most abundant, followed by ethylene, vinyl radical, and acetylene. Hydrocarbons containing three carbons (e.g., propane, propene, and propyl) were minor products, and only a few molecules containing four carbon atoms (e.g., iso-butene, 1-methylpropylidene, and 2-buten-2-yl) formed. Products that can be formed from the reaction of 1−3 impact fragmentation events, ethane, ethyl radical, and ethylene, monotonically increased over time, while products of 3 or more impact fragmentation events, vinyl, propane, and acetylene, formed over longer time scales. The number of methane complexes decreased over time. For a methane/water (1:1) ice mixture, most of the products consisted of methyl−water complexes, and their number increased with time. All the other oxygenated and nonoxygenated products formed in small amounts due to the water solvation of radicals. For a methane/water (4:1) ice mixture, the methyl−water complexes constituted 45% of the total products, with oxygenated and nonoxygenated products being formed in almost equal amounts. For methane−water ices, the proportions of alkanes, alkenes, and alkynes were very similar to those of pure methane. Dimethyl ether and ethanol formed for both 1:1 and 4:1 methane−water ices.

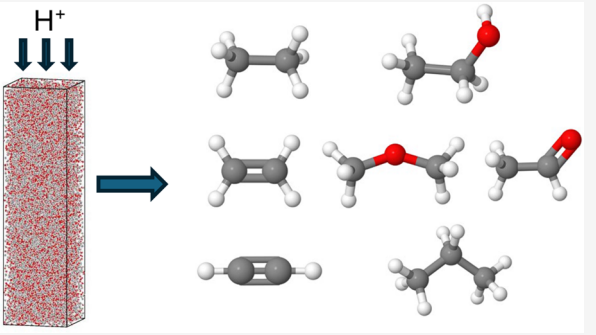

KEYWORDS: *solar wind irradiation, molecular dynamics, reactive chemistry, ices, complex organic molecules*

1. INTRODUCTION

Solid methane was detected toward young stars in molecular clouds[1] and was also identified in the diffuse interstellar medium (ISM) along the line of sight toward Sgr A* and the Quintuplet sources GCS 3 and GCS 4.[2,3] Methane−water ices are ubiquitous in many interstellar and circumstellar environments,[4−6] such as protostellar objects,[7−10] low-mass young stellar objects,[11] and cometary ices.[12] In the Solar System, methane ice can be detected either pure or mixed with other volatiles on the surface of planets and their satellites.[13] In the outer Solar System, solid methane has been detected on the surface of the Kuiper Belt Objects (KBOs), such as Triton, Eris, Pluto, Makemake, Sedna, Orcus, Quaoar, and 2007 OR_{10} in conjunction with other ices, such as H_2O and N_2.[14] The presence of surface areas containing pure solid methane has been confirmed for Pluto,[15] Eris,[16] and Quaoar.[14]

Ices on the surface of KBOs that lack an atmosphere are exposed to solar wind ions, solar energetic particles, galactic cosmic rays (GCRs), and UV photons.[17−21] Fast ions deposit energy in the ices via elastic and inelastic collisions that induce excitations and ionizations and lead to the formation of vibrationally excited radicals and atoms with an excess of kinetic energy. These reactive species react to form new complex organic molecules (COMs) containing six atoms or more and with at least one carbon.[22] Recent James Webb Space Telescope (JWST) observations of Trans-Neptunian Objects and Centaurs have revealed the presence of volatile ices, such as ethane (C_2H_6), acetylene (C_2H_2), and ethylene (C_2H_4) on the surface of Sedna, ethane on the surface of Quaoar,[23] and ethane, propane (C_3H_8), and acetylene on the surface of Chiron.[24] As the irradiation dose increases from tens to hundreds of eV/molecule, the complexity of the molecules formed increases eventually producing an organic residue.[25,26]

Received: August 6, 2024
Revised: November 18, 2024
Accepted: November 22, 2024
Published: December 2, 2024

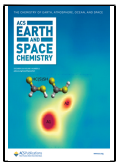

https://doi.org/10.1021/acsearthspacechem.4c00225
ACS Earth Space Chem. 2024, 8, 2509−2521

This residue may evolve into a form of amorphous carbon at even higher doses.[27,28]

MeV proton irradiation experiments have been performed on methane ice targets to simulate the interaction of GCRs with organic ices and the production of new molecules.[29] Using Fourier transform infrared (FTIR) spectroscopy to monitor the solid phase and quadrupole mass spectrometry (QMS) to monitor the gas phase, they detected acetylene (C_2H_2), ethylene (C_2H_4), ethane (C_2H_6), as well as vinyl (C_2H_3), ethyl (C_2H_5), carbene (CH_2), and methyl (CH_3) radicals in the ice. To simulate the effect of secondary electrons released in the tracks of MeV protons, methane ices were irradiated using 5 keV electrons, and the experiments were monitored using FTIR in the solid phase and QMS coupled with electron impact ionization (EI) to monitor species in the gas phase. Similar species to those obtained using MeV protons were identified, namely, methyl radical, ethane, ethyl radical, ethylene, vinyl radical, and acetylene.[30] While FTIR is effective at detecting small molecules in the solid phase, it is not capable of identifying large more complex molecules due to overlapping absorption bands. Moreover, the QMS/EI approach has limitations due to the extensive fragmentation of EI that makes it challenging to discriminate between isomers. To overcome these limitations, reflectron time-of-flight mass spectrometry coupled to soft ionization (PI-ReTOF-MS) has been used to identify molecules that sublime into the gas phase during temperature-programmed desorption. Using methane as a case study, hydrocarbons with up to 22 carbons and containing alkanes, alkenes, alkynes/dienes, and aromatic hydrocarbons were detected after electron irradiation.[31,32]

Irradiation experiments of methane−water ices with ratios of 1:2, 1:7, and 1:15 using 1 MeV protons have shown that the amount of ethane formed is related to the amount of methane initially present.[33] Ethane, methanol (CH_3OH), ethanol (CH_3CH_2OH), carbon monoxide (CO), carbon dioxide (CO_2), formaldehyde (H_2CO), acetaldehyde (CH_3CHO), and propane (C_3H_8) were identified using FTIR spectroscopy, with ethane, methanol, and ethanol having the highest concentrations, and acetylene was not detected. Subsequent irradiation experiments of methane−water ices with a ratio of 5:2 using 1 MeV protons produced acetylene in addition to ethane, propane, methanol, carbon monoxide, carbon dioxide, and probably formaldehyde.[34] Recent laboratory irradiation studies of methane-water ices with a ratio of 1:9 using 5 keV electrons using PI-ReTOF-MS and FTIR have allowed the identification of isomers with masses between 40 and 56 amu. For species with masses between 56 and 100 amu, conclusive assignments could not be made based on the large number of possible isomers, and plausible candidates were suggested.[35,36] These new results illustrate the complexity of the chemistry involved and the need for theoretical simulations to help interpret the laboratory results.

Different theoretical approaches have been developed to simulate the chemical changes induced by the ionizing radiation of astronomical ices. Rate-equation-based astronomical models have been extended to explicitly include the effects of radiolysis.[37−39] Monte Carlo simulations of GCR protons with energies of MeV−GeV have been performed using the Geant4-DNA code[40] to model the processes occurring in the GCR ion tracks. The impacts of solar wind protons on icy surfaces have been modeled using molecular dynamics (MD) and the reactive force field ReaxFF,[41] which allows for the formation and breaking of bonds.[42] Single-impact simulations with 0.829 keV protons lead to the formation of only a few products. It was necessary to use 16.8 keV Ne^{2+} ions to produce more molecules.

In this paper, we present a new MD approach to simulate the chemistry involved in the irradiation of ices by solar wind protons and the formation of COMs. We use the mixed methane−water and pure methane ice cases to showcase our results, and we compare them to previous experiments.

2. METHODS

Previous MD simulation studies of solar wind ion impacts using H, He, and Ne were geared toward the interrogation of ion-initiated radicalization of ice species and the resulting early-stage chemical reactions.[42] Those simulations showed that it was necessary to increase the ion mass to form larger amounts of molecules, including complex molecules, due to the greater nuclear energy deposited in the material. Impacts of a single proton were performed once or repeated multiple times. Their results showed that increasing the number of impacts led to an increase in product formation.

The present impact approach was developed with the intention of accelerating reactions to obtain more statistics on early-stage radicalization events and long-time reactions that lead to larger molecular weight products using H instead of Ne ions given that they are the predominant species in the solar wind. We use seven 0.829 keV H^+ (total energy of 5.8 keV), with a velocity of 400 km/s, impacting the surface simultaneously to increase the fluence (ions cm^{-2}), and we repeat the impact simulation over an arbitrary number of impact cycles to mimic a continuous ion bombardment of the surface and to maximize the formation of complex intermediates and products. The proton impactors can transfer energy to the ice through both elastic nuclear collisions and inelastic energy that is distributed to atoms around the impact track. The energy of the impactors is low enough to prevent sputtering from occurring in our simulations. The sputtering yield for H^+ has a quadratic dependence on the electronic stopping power of the projectile.[43,44]

Details of the model and its application to various ice systems through MD simulations are provided in the following subsections.

2.1. Impactor−Target Systems. The present study focuses on the influence of H^+ impacts on species formation in two target ices—pure CH_4 and two CH_4:H_2O mixtures with ratios of 1:1 and 4:1. PACKMOL[45] was used to construct molecular models of the ice systems. For the CH_4 ice system, we used a cell with dimensions 55 × 55 × 220 Å along the *x*, *y*, and *z* directions, containing 20,494 methane molecules. The system's temperature was first set to 300 K and then cooled to 1 K using a Berendsen thermostat. To the final system, an additional 10 Å of vacuum space was added in the direction of proton impact (*z*-direction), resulting in a final z dimension of 230 Å.

For the CH_4:H_2O 1:1 mixture, we first determined its density using a cell with dimensions 55 × 55 × 200 Å along the *x*, *y*, and *z* directions, containing 8561 CH_4 and 8561 H_2O molecules, and with a density of 0.8 g/cm^3. The positions were first evolved in the canonical ensemble, with constant number, volume, and temperature (NVT) at 300 K for 5 ps, followed by a cool down from 300 to 1 K, and finally evolved in the isothermal−isobaric ensemble (NPT) at 1 K and ambient pressure for 10 ps. The density converged to 0.82 g/cm^3 and to 8775 CH_4 and 8775 H_2O molecules. We generated the final

https://doi.org/10.1021/acsearthspacechem.4c00225
ACS Earth Space Chem. 2024, 8, 2509−2521

system using this density, and an additional 20 Å of vacuum space was added in the direction of proton impact (z-direction), resulting in a final z dimension of 220 Å.

The same approach used for the 1:1 CH_4:H_2O case was used for the 4:1 case. We first determined its density using a cell with dimensions 55 × 55 × 200 Å along the x, y, and z directions, containing 12,416 CH_4 and 3104 H_2O molecules, and with a density of 0.7 g/cm^3. The density converged to 0.66 g/cm^3 and to 11,708 CH_4 and 2927 H_2O molecules. We generated the final system using this density and an additional 20 Å of vacuum space was added in the direction of proton impact (z-direction), resulting in a final z dimension of 220 Å. To the final structures, seven protons were initialized in random positions on the x−y plane 10 Å above the surface before running impact simulations (Figure 1).

2.2. Multiproton Impact Simulations. Impact simulations were initialized by providing the seven H^+s, impacting the surface along the z direction with a velocity of 400 km/s (i.e., 4 Å/fs; 829 eV/proton) that corresponds to the speed at max flux of the solar wind. The dose was calculated as the total energy (in eV) deposited in the system per molecule and computed by multiplying 829 eV by the number of H^+ impacts. Positions of the impacting protons were evolved in the microcanonical ensemble, with constant number, volume, and energy (NVE). Interactions between the protons and ice species were represented using a reactive force field (ReaxFF),[46] which allowed molecular dissociation from the interaction with impacting protons and the subsequent reaction and formation of new species from the fragments. A small time step of 0.01 fs was used to ensure energy conservation and full resolution of the dynamics between ice molecules and the high-velocity protons. To mimic an extended target and prevent scattered protons or fragments from passing through periodic boundaries, a damped boundary condition was applied in all the periodic directions. The damping was computed as $-\gamma v$, where γ is a damping constant set to 50 eV fs/Å^2 and v is the velocity of the ion.

Additionally, the simulations accounted for electronic stopping, computed as energy loss of the H^+ impactors as a function of velocity, or $F = -kv$, where k is the friction parameter and v is the velocity. We used the code SRIM (Stopping and Range of Ions in Matter)[47] to determine the value of k for a given ice mixture with a given density. The electronic stopping parameters used were 0.32 and 0.57 eV fs/Å for CH_4:H_2O and CH_4 ice, respectively. The kinetic energy of the H^+ lost from electron stopping leads to electronic excitation of molecules neighboring the proton trajectory through inelastic collisional effects. These effects are approximated by distributing proton kinetic energy lost from electron stopping to neighboring ice molecules with the energy being distributed equally to all species within 0.6 nm, the radius of methane, of the proton. This choice of distribution radius can be rationalized based on studies that have investigated the spatial extent of inelastic energy transfer in 0.1−100 MeV proton impacts of ices computationally, finding the energy to be distributed up to 9.9−8.4 nm away from the proton.[40] Although explicit simulations of protons in the range of interest here (0.008 MeV) were not treated in that work, an extrapolation of the available data down to this energy level provides an approximated <1 nm distribution radius.

To simulate a continuous ion bombardment of the ice that would be present in laboratory experiments and solar wind, multiple impact cycles are performed on the ice target. Each impact cycle is defined to last 50,000 timesteps, or 0.5 ps, which was shown in previous work to be a sufficient time for any product, resulting from H^+ impacts of the ice to form and stabilize.[42] At the start of each cycle, the impacting protons are

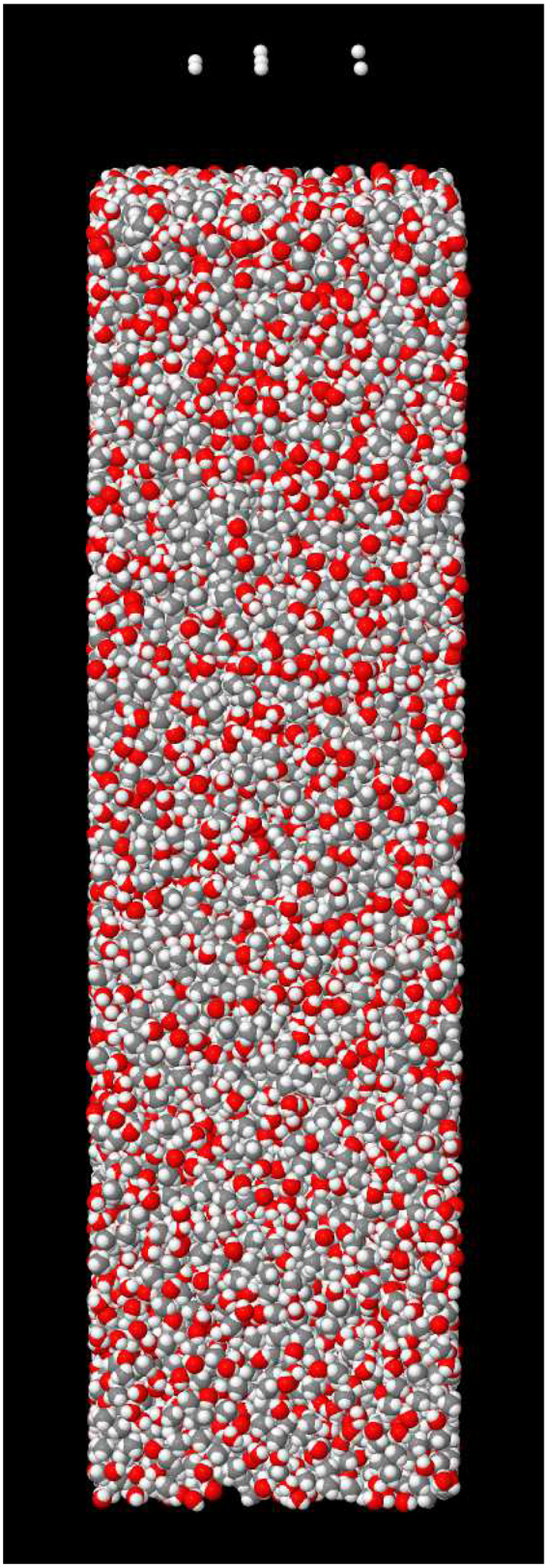

Figure 1. Box containing a CH_4:H_2O (1:1) ice mixture with 7 H^+ above the surface.

https://doi.org/10.1021/acsearthspacechem.4c00225
ACS Earth Space Chem. 2024, 8, 2509−2521

reinitialized by resetting their positions to the surface of the ice and their velocities to a starting value of 400 km/s. This can be performed for an arbitrary number of cycles, allowing deposition of a sufficient dose of energy over long enough times to observe the formation of nontrivial products. Concurrently, resetting the protons prevents the accumulation of protons in the material, which is undesired for the present simulations of near-surface ice reactions due to the impacts. To avoid excessive heating and sublimation of the ices, temperature control was imposed after each impact cycle to quench the system by rescaling the velocities to 15 K. The system with reinitialized proton positions and velocities was then used as the starting point for the next impact cycle.

2.3. MD Simulation Details. MD simulations were performed with LAMMPS (Large-scale Atomic/Molecular Massively Parallel Simulator),[48] an open-source code from Sandia National Laboratories, which has been modified to handle multiple H^+ impacts by creating a new fix called "impact". The energetics of the proton-ice systems were described by the ReaxFF functional form of Chenoweth et al.,[46] with protons being excluded from the charge equilibration procedure associated with ReaxFF. The ReaxFF parameters used included the recent potential of Zhang and van Duin[49] to describe the CH_4:H_2O ice mixture as it accurately describes weak interactions, such as hydrogen bonds, and the potential from Chenoweth et al.[46] (field.reax.-cho in LAMMPS), which is well-suited for pure hydrocarbons, to study the methane ice. ReaxFF does not fully account for the repulsive forces associated with high-energy proton−atom elastic collisions. Thus, the Ziegler−Biersack−Littmark (ZBL) potential was added to correctly represent energetics of close atomic approaches.[50] The ZBL potential adds a "hard" repulsive force at small atomic distances and has been applied to successfully describe impact in previous studies.[42,51]

2.4. Molecular Product Detection. The molecules were identified by visualizing the atomic coordinates using the freely available JMol software. For each atom, a list of bonds was created using the distance between each pair of atoms (NB: periodic boundary conditions were accounted for in this process). Starting from an atom, its neighbors were determined, then the neighbors of the neighbors, then the neighbors of the second neighbors, and so on until all of the atoms in the molecule were identified. The atoms in the molecule were removed from the pool of available atoms. A new atom was chosen, and the process was repeated until all of the atoms were considered.

3. RESULTS

3.1. Impact and Reaction Characteristics. The protons impacting the system can transfer energy through both elastic scattering via nuclear collisions and inelastic electron stopping. In the electron stopping limit, with no elastic collisions, velocity as a function of time is represented as

$$v(t) = v_0 e^{-k/mt} \quad (1)$$

where v_0 is the initial velocity and m is the mass of the impacting proton. An examination of the average proton velocities as a function of time (Figure 2) from the simulation to the electron stopping limit shows the significant influence of elastic scattering. In both CH_4:H_2O and CH_4 ice systems, the proton slows significantly within 100 fs before traveling the length of the simulation box and being slowed down by the damping boundary conditions to zero velocity.

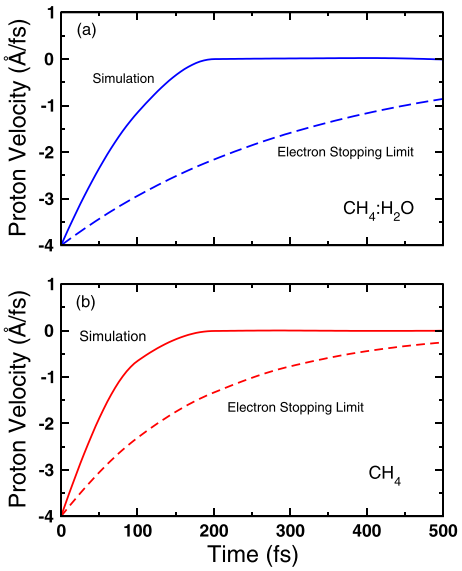

Figure 2. Average velocity of impacting protons as a function of time, along with the ideal electron stopping limit, which assumes only inelastic deceleration for (a) CH_4:H_2O and (b) CH_4 ices.

The proton impacts lead to the formation of molecular fragments, which can subsequently react. The ratio of fragmented or reacted molecules to pristine molecules can be tracked as a function of time as impacts proceed (Figure 3).

For the CH_4:H_2O system, roughly a third of all molecules undergo a fragmentation or reaction process within 8 ps or 112 proton impacts. On the other hand, for the CH_4 system, fragmentation and reaction occurs more slowly, taking roughly three times longer than in the CH_4:H_2O system (Figure 3a,b).

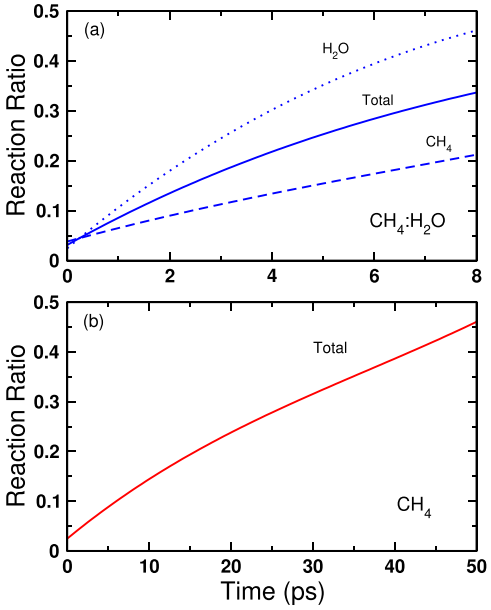

Figure 3. Ratio of molecules that have undergone fragmentation or reaction in (a) CH_4:H_2O ice while receiving a dosage of 5.7 eV/molecule over 8 ps and (b) CH_4 ice while receiving a dosage of 28.4 eV/16u after 50 ps. For CH_4:H_2O, the ratios of H_2O and CH_4 are shown along with the total.

https://doi.org/10.1021/acsearthspacechem.4c00225
ACS Earth Space Chem. 2024, 8, 2509−2521

The difference in behavior can be attributed to the stabilization of the products by polar water molecules. This applies to both ionic species formed from impacts like OH^-, H^+, and H_3O^+, as well as radical products of CH_4.

To this point, at any given time during the impact simulation, the CH_4:H_2O ice has a higher relative reaction ratio of CH_4 compared to pure CH_4 ice (Figure 3a,b). A visual representation of the extent of the reaction for the CH_4 ice system (Figure 4) shows that reactions uniformly occur throughout the systems. More details of species evolved from fragmentation products are examined in the following subsections.

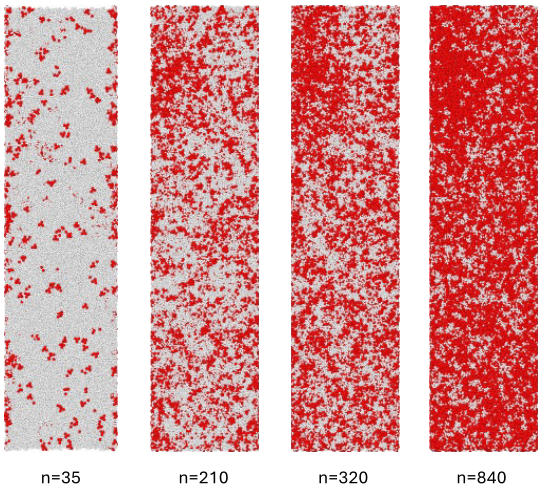

Figure 4. Depiction of the extent of molecular fragmentation and reaction in the methane ice system after being impacted by *n* protons. White particles represent pristine methane molecules, while red particles represent methane molecules that have undergone fragmentation or reaction.

3.2. Irradiation of the CH_4 Ice. *3.2.1. Molecules Formed by Radiolysis.* We have run one MD simulation for 73 ps with a total of 1029 H^+ impacts and a total dose of 41.6 eV/16u. Our total dose is comparable to estimates of 25 eV/16u[52] and 60 eV/16eu[53] on Pholus' surface. The H^+ impacts lead to the formation of a large number of radicals and atoms derived from the H abstraction from methane, namely, CH_3 (3033), CH_2 (301), CH (17), and C (0). H_2 molecules (2442) formed by recombination of H radicals and free H radicals (885) were remaining. A fraction of these radicals reacted to form a total of 613 new, more complex molecules (see Table 1). The structures of all of the molecules formed are shown in Figure 5.

Ethane (structure 1), ethyl radical (structure 2), ethylene (structure 15), vinyl radical (structure 16), acetylene (structure 18), and propane (structure 7) were the dominant products formed in our simulations, and their detection was also obtained in previous experiments.[29,30,32,54,55] The methyl radical was produced experimentally, which we also formed in our simulations. We also obtained a complex of the methyl radical with methane via the H atom (structure 5). To compare with laboratory experiments, we use the results for a dose of 2.8 eV/16au and a simulation length of 5 ps. In Table 2, we compare the relative abundances of the dominant complex products formed in our simulations with previous laboratory experiments.[30,32] Ethane is formed in the largest quantity in both experiments and in our work. Our relative abundances for ethylene and acetylene are comparable to those obtained by Abplanalp et al.[32] and for vinyl to those from Bennett et al.[30] The major difference is for ethyl, which is more abundant in our simulations, as illustrated by its temporal evolution (see Section 3.2.2).

Table 1. Summary of the Number of Hydrocarbon Molecules (See Figure 5) Formed in the Proton Bombardment Simulation of the CH_4 Ice

molecule	formula	number
1	CH_3-CH_3	267
2	CH_3-CH_2	120
3	CH_3-CH	14
4	CH_3-C	1
5	CH_3-H-CH_3	3
6	CH_3-H-CH_2	1
7	$CH_3-CH_2-CH_3$	23
8	$CH_3-CH_2-CH_2$	9
9	CH_3-CH_2-CH	1
10	$CH_2CH_2CH_2$	2
11	$CH_3-CH-CH_3$	6
12	CH_3-C-CH_3	2
13	$CH_3-CH_2-C-CH_3$	2
14	$(CH_3)_3CH$	1
15	$CH_2=CH_2$	69
16	$CH_2=CH$	55
17	$CH_2=C$	2
18	$CH\equiv CH$	13
19	$CH\equiv C$	2
20	$CH_3-CH=CH_2$	10
21	$CH_3-C=CH_2$	3
22	$CH_3-CH=C-CH_3$	1
23	$CH_2=C=CH_2$	2
24	$CH_2=C=CH$	1
25	$CH_2=CH=CH_2$	2
26	$CH_2=CH_2-C\equiv CH$	1
total	613	

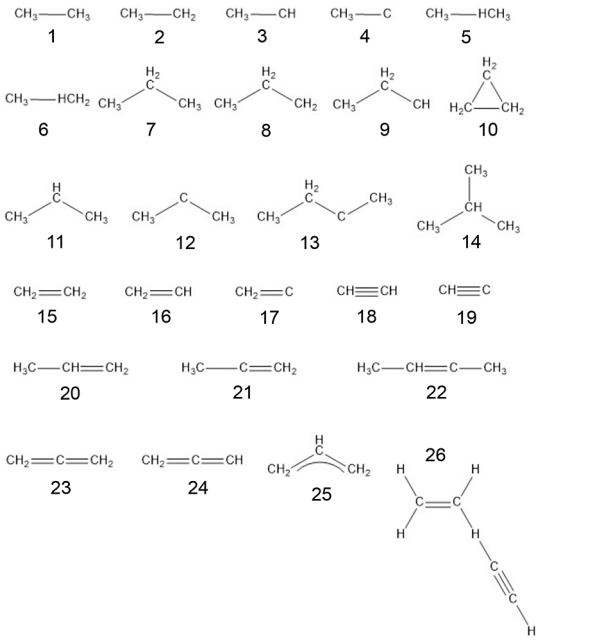

Figure 5. Structures formed in the simulations of proton bombardments of the CH_4 ice.

https://doi.org/10.1021/acsearthspacechem.4c00225
ACS Earth Space Chem. 2024, 8, 2509−2521

Table 2. Comparison of the Relative Abundances (Relative to Ethane) of the Dominant Complex Products Formed by Irradiation of the CH_4 Ice as a Function of Projectile Type, Energy/Particle (keV), and Dose/16u

this work					previous work[a,b]					
mol.	proj.	E	dose	rel. ab.	proj.	E	dose		rel. ab.	
ethane	H^+	5.8	2.8	1.0	e^-	5.0[a,b]	1.6[a]	3.5[b]	1.0[a,b]	
ethylene	H^+	5.8	2.8	0.17	e^-	5.0[a,b]	1.6[a]	3.5[b]	0.32[a]	0.25[b]
ethyl	H^+	5.8	2.8	0.42	e^-	5.0[a,b]	1.6[a]	3.5[b]	0.09[a]	0.05[b]
vinyl	H^+	5.8	2.8	0.08	e^-	5.0[a,b]	1.6[a]	3.5[b]	0.02[a]	–[b]
acetylene	H^+	5.8	2.8	0.08	e^-	5.0[a,b]	1.6[a]	3.5[b]	0.05[a]	0.09[b]

[a]Bennett et al.[30] [b]Abplanalp et al.[32]

We also formed propene (structure 20), which was formed in VUV experiments,[56] and allene (structure 23), which was detected in microwave discharge hydrogen flow lamp experiments.[57] Experiments using 5 keV electrons, along with the PI-ReTOF-MS and FTIR detection methods, have allowed the detection of *n*-butane (C_4H_{10}) and larger hydrocarbons with up to 22 carbons.[31,32] In our simulations, we obtained the 1-methylpropylidene radical (structure 13), a precursor of *n*-butane and iso-butane (C_4H_{10}) (structure 14), which was formed in VUV experiments.[56] We also formed a complex between vinyl and acetylene (structure 26).

Several intermediate radicals were formed in our simulations: methylcarbene (structure 3), vinylidene (structure 4), propyl (structure 8), ethylcarbene (structure 9), isopropyl (structure 11), ethylidene, 1-methyl (structure 12), 1-methylpropylidene (structure 13), vinyl (structure 16), vinylidene (structure 17), ethynyl (structure 19), 2-propenyl (structure 21), 2-buten-2-yl (structure 22), allenyl (structure 24), and allyl (structure 25).

Figures 6 and 7 show that our simulations of pure methane produce very similar breakdowns of alkanes, alkenes, and alkynes, as for the cases of CH_4:H_2O (1:1) and (4:1).

3.2.2. Temporal Evolution of Molecular Formation. The temporal evolutions of the main products formed during the irradiation of CH_4 are shown in Figure 8. We include data for ethane (structure 1), ethyl radical (structure 2), ethylene (structure 15), vinyl radical (structure 16), propane (structure

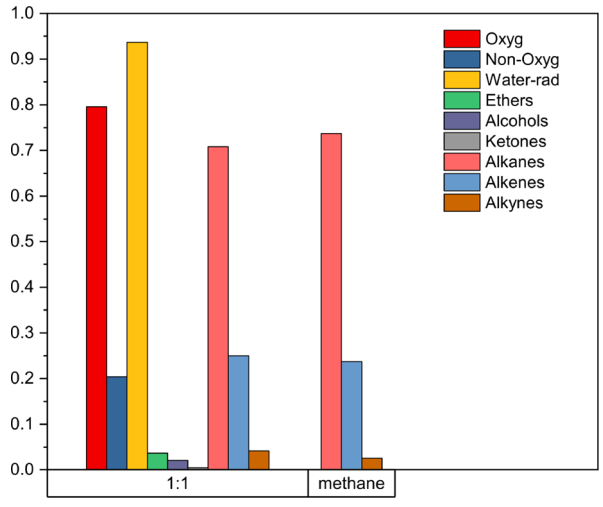

Figure 6. Histograms illustrating the fractions of total oxygenated versus total nonoxygenated molecules, the types and fractions of oxygenated and nonoxygenated (C, H only) molecules formed in the CH_4:H_2O (1:1) simulations (average over the 7 runs) and in the pure CH_4 simulations.

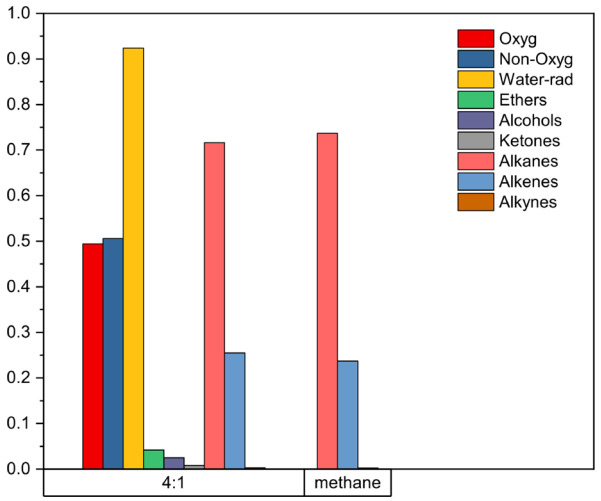

Figure 7. Histograms illustrating the fractions of total oxygenated versus total nonoxygenated molecules, the types and fractions of oxygenated and nonoxygenated (C, H only) molecules formed in the CH_4:H_2O (4:1) simulations (average over the 7 runs) and in the pure CH_4 simulations.

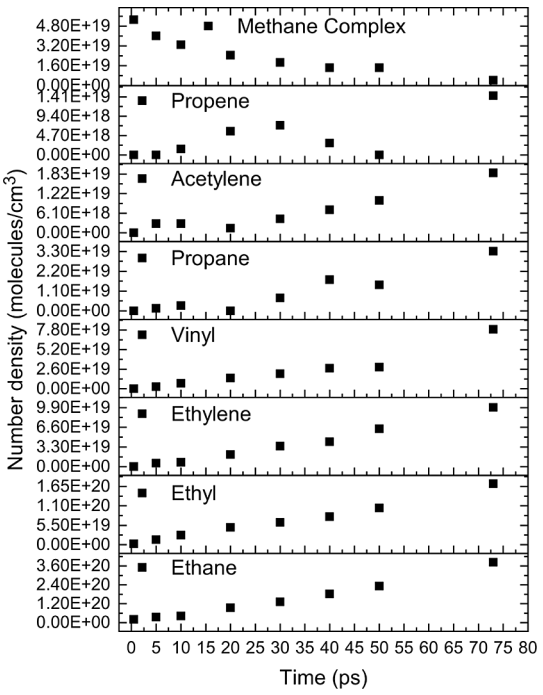

Figure 8. Number density of molecules formed as a function of time in simulations of proton bombardments of the CH_4 ice. The range of values for the *y*-axis varies for each molecule.

https://doi.org/10.1021/acsearthspacechem.4c00225
ACS Earth Space Chem. 2024, 8, 2509−2521

7), acetylene (structure 18), propene (structure 20), and the methane complex (structure 5).

Methane complexes form during the first couple of impacts. As the irradiation time increases, the number of methane complexes decreases exponentially to almost zero after 73 ps, as opposed to the number of larger hydrocarbon products, which increases with time. Products that can be formed from the reaction of 1−3 impact fragmentation events, ethane, ethyl radical, and ethylene, monotonically increase in time, while products of 3 or more impact fragmentation events, vinyl, propane, and acetylene, form over longer time scales. The temporal evolution of propene reaches a maximum at around 30 ps before decreasing to negligible concentrations at longer times, consistent with propene being an intermediate species. The temporal evolutions obtained by Abplanalp et al.[32] (see Figure 16 in Abplanalp et al.) indicate that, experimentally, the formation of ethylene is monotonic, whereas that of ethyl grows asymptotically and reaches a column density of an order of magnitude smaller than that of ethylene.

3.3. Irradiation of the CH_4:H_2O (1:1) Ice. We have performed seven series of simulations, as listed in Table 3, for doses ranging from 6.0 to 10.3 eV/molecule, which are smaller than the estimates of 25 eV/16u[52] and 60 eV/16u[53] on Pholus' surface.

Table 3. Summary of the Proton Bombardment Simulation Runs for the CH_4:H_2O (1:1) Ice

run	number of impacts	molecules formed	length of simulation (ps)	dose (eV/molecule)
1	175	241	11.6	8.3
2	175	276	11.7	8.3
3	210	293	12.8	9.9
4	147	217	9.3	6.9
5	217	314	14.5	10.3
6	168	201	10.2	7.9
7	126	172	7.7	6.0

3.3.1. Molecules Formed by Radiolysis. The structures of all the complex molecules formed in the 7 series of simulations are shown in Figure 9. In Table 4, we list the number of hydrocarbon (nonoxygenated) molecules for each run, and in Table 5, we list the number of oxygenated molecules for each run.

The breakdown of each class of molecule (e.g., alkanes, alkenes, alkynes, ethers, alcohols, and ketones) is shown in Figure 6. Table 4 shows that the dominant stable hydrocarbon (nonoxygenated) product is ethane (C_2H_6, structure 1), with an average of 23 molecules formed, followed by ethylene (C_2H_4, structure 15), with an average of 6 molecules produced. Minor hydrocarbons formed are acetylene (C_2H_2, structure 18), with an average of two molecules formed, and propane (C_3H_8, structure 7).

Irradiation experiments of methane−water ices with ratios of 1:2, 1:7, and 1:15 using 1 MeV protons have shown that ethane is a major product, and propane is a minor product. The amount of ethane formed is related to the amount of methane initially present. Increasing the amount of water decreases the amount of ethane as it forms more readily when a CH_3 radical is next to another CH_3 radical as opposed to a water molecule or an OH radical. For a methane−water ratio of 1:2, an ethane/propane ratio of 4.9 was obtained for a dose of 17 eV/molecule.[33] Ethane was also produced in the

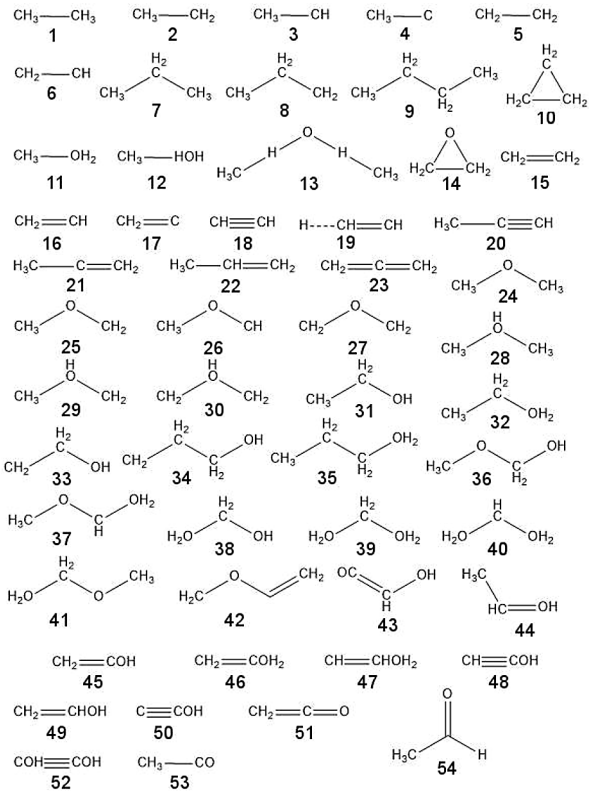

Figure 9. Structures formed in the proton bombardment simulation runs of the CH_4:H_2O (1:1) ice.

irradiation of methane−water ice with a ratio of 1:4 at 12 and 40 K using 30 keV He^+ ions.[58] In recent irradiation experiments of methane−water ice with a ratio of 5:2, ethane, propane, and acetylene were formed using 1 MeV protons, but acetylene did not form when 2 keV electrons were used.[34] In our simulations, after an average dose of 8 eV/molecule, ethane was the dominant product, with propane as a minor product (ethane/propane ratio of 11.5).

Table 5 shows that dimethyl ether (CH_3OCH_3, structure 24) and ethanol (CH_3CH_2OH, structure 31) were the most common oxygenated products, with an average of 4 and 3 molecules formed, respectively. Methyl (CH_3) radicals formed complexes with water, such as $CH_3(H_2O)$ and $(CH_3)_2H_2O$ (see structures 11, 12, and 13). Methanol could form from these complexes by hydrogen abstraction reactions. The acetyl radical (CH_3−C═O, structure 53), a precursor of acetaldehyde (CH_3CHO), was only formed in selected runs.

Irradiation experiments of methane−water ices with ratios of 1:2, 1:7, and 1:15 using 1 MeV protons formed methanol (CH_3OH), ethanol (CH_3CH_2OH), carbon monoxide (CO), carbon dioxide (CO_2), formaldehyde (H_2CO), and acetaldehyde (CH_3CHO). For a methane−water ratio of 1:2, methanol and ethanol were formed in comparable amounts and acetaldehyde was an order of magnitude less abundant.[33] The relative abundance of CO and CO_2 with respect to the initial amount of methane molecules was ≈1%.[33,58] Methanol, carbon monoxide, carbon dioxide, and formaldehyde were also formed in other proton irradiation experiments of methane−water ices.[34,58] Ethanol and dimethyl ether were identified using the PI-ReTOF-MS detection method.[35,36]

Table 6 shows the number of molecules per run, along with the averages of H, H_2, OH, O_2, and CO and CO_2. The

https://doi.org/10.1021/acsearthspacechem.4c00225
ACS Earth Space Chem. 2024, 8, 2509−2521

Table 4. Summary of the Number of Hydrocarbon Molecules (See Figure 9) Formed in Each Proton Bombardment Simulation Run of the CH_4:H_2O (1:1) Ice, Along with the Averages

molecule	formula	run 1	run 2	run 3	run 4	run 5	run 6	run 7	ave
1	CH_3-CH_3	19	27	30	24	27	18	17	23
2	CH_3-CH_2	6	9	10	10	13	5	5	8
3	CH_3-CH	3	3	2	3	0	2	0	2
4	CH_3-C	0	0	0	1	0	0	1	0
5	CH_2-CH_2	0	0	1	0	0	0	0	0
6	CH_2-CH	0	1	0	0	0	0	1	0
7	$CH_3-CH_2-CH_3$	2	2	0	2	0	0	0	1
8	$CH_3-CH_2-CH_2$	0	0	0	0	1	0	0	0
9	$CH_3-CH_2-CH_2-CH_3$	0	0	0	0	0	1	0	0
10	$CH_2-CH_2-CH_2$	0	0	1	0	0	0	0	0
15	$CH_2=CH_2$	5	8	9	2	8	6	3	6
16	$CH_2=CH$	5	7	8	5	7	4	5	6
17	$CH_2=C$	1	0	0	0	0	0	0	0
18	$CH\equiv CH$	4	3	0	2	1	0	2	2
19	$H-CH=CH$	0	1	0	0	0	0	0	0
20	$CH_3-C\equiv CH$	0	0	0	0	0	1	0	0
21	$CH_3-C=CH_2$	0	0	0	0	0	1	0	0
22	$CH_3-CH=CH_2$	0	0	1	0	0	2	0	0
23	$CH_2=C=CH_2$	0	0	1	1	0	0	0	0
total		45	61	63	50	57	40	34	50

dominant products are H (423) and H_2 (526) with OH (7) and CO (3) being minor products. O_2 and CO_2 form only in some simulation runs. The formation of CO, CO_2, and O_2 requires total loss of H from carbon and oxygen; given the doses and time scales in our simulations, it is not surprising that they form in small amounts. Several intermediates and products formed in our simulations could potentially form H_2CO with more impacts.

Additional stable closed-shell molecules were produced in some of our simulation runs, which were not detected in the proton irradiation experiments discussed above. Many of these molecules were obtained in experiments using 5 keV electrons, along with the PI-ReTOF-MS and FTIR detection methods.[35,36,59,60]

We should note that PI-ReTOF-MS is an indirect analytical technique. The ice obtained upon irradiation with the electrons is warmed until desorption of its components into the gas phase. This can involve chemical alteration of the ice through thermal processing. Molecules in the gas phase experience collisions with the walls of the setup and are ionized before being admitted to TOF-MS. Upon ionization, ions may experience isomerization and further chemical alteration. This analysis can only give indirect information about the composition of the ice. For example, all the complexes and free radicals obtained upon irradiation of the ice in the simulations will participate in various chemical reactions upon warming or be decomposed.

For molecules with m/z = 40, our simulations produced the isomers methylacetylene (structure 22) and allene (structure 19). Methylacetylene was detected in the PI-ReTOF-MS experiments.

For molecules with m/z = 42, our simulations formed the isomers propene (structure 22), cyclopropane (structure 10), ketene (structure 51), and ethynol (structure 48). Propene, ketene, and ethynol were identified in the PI-ReTOF-MS experiments. Ketene was recently identified by synchrotron vacuum ultraviolet photoionization reflectron time-of-flight mass spectrometry (SVUV-PI-ReTOF-MS).[61]

For molecules with m/z = 44, we obtained acetaldehyde (structure 54) and vinyl alcohol (structure 49), which were also confirmed in the PI-ReTOF-MS experiments. Acetaldehyde and vinyl alcohol were also identified using SVUV-PI-ReTOF-MS.[61] We also formed ethylene oxide (structure 14) and propane (structure 7).

For molecules with m/z = 46, we obtained ethanol and dimethyl ether, as already discussed above.

For molecules with m/z = 58, we formed n-butane (structure 9) and acetylenediol (structure 52). We also formed methoxymethanol (structure 36) with m/z = 62 and ethenone hydroxy (structure 43).

In addition to these stable molecules, we also formed intermediate radical species. It has been postulated that, in addition to the methyl radical, suprathermal C, CH, and CH_2 species form upon irradiation of methane ices by MeV protons and can undergo insertion reactions to form radicals, such as methylcarbene (CH_3CH) and ethyl radical (CH_3CH_2).[29] Larger radicals are predicted to form by subsequent insertion, addition, and abstraction reactions.

The most common C_2H_y radicals formed in our simulations were ethyl (structure 2), methylcarbene (structure 3), and vinyl radical (structure 16), in agreement with previous laboratory results.[29] In selected runs, we also formed vinylidyne (structure 4), triplet ethylene (structure 5), ethenyl (structure 6), and ethenediide (structure 19). The only C_3H_y radical formed was 2-propenyl radical (structure 21).

In addition to pure (C,H only) radicals, we also formed oxygen-containing radicals. The most common radicals formed were methoxymethyl (structure 25), hydrogenated methoxymethyl (structure 29), 1-hydroxyethyl (structure 44) and ethenyl, 1-hydroxy (structure 45). Minor oxygen-containing radicals were produced in a few selected runs and included methoxycarbene (structure 26), methoxymethane (structure 27), protonated dimethyl ether (structure 28), protonated methoxymethane (structure 30), ethyl, 2-hydroxy (structure 33), 3-hydroxypropyl (structure 34), (vinyloxy)methane

https://doi.org/10.1021/acsearthspacechem.4c00225
ACS Earth Space Chem. 2024, 8, 2509−2521

Table 5. Summary of the Number of Oxygen-Containing Molecules (See Figure 9) Formed in Each Proton Bombardment Simulation Run of the CH_4:H_2O (1:1) Ice, Along with the Averages

molecule	formula	run 1	run 2	run 3	run 4	run 5	run 6	run 7	ave
11	$CH_3-(OH_2)$	177	188	198	148	227	139	118	171
12	$CH_3-(HOH)$	3	6	6	2	3	2	6	4
13	$(CH_3)_2H_2O$	0	0	1	0	0	0	0	0
14	CH_2OCH_2	0	0	1	0	0	0	0	0
24	CH_3-O-CH_3	7	5	6	2	4	5	0	4
25	CH_3-O-CH_2	4	1	3	3	4	0	0	2
26	CH_3-O-CH	0	0	0	0	1	0	0	0
27	CH_2-O-CH_2	0	1	0	0	0	0	0	0
28	$CH_3-(OH)-CH_3$	0	0	0	1	0	2	0	0
29	$CH_3-(OH)-CH_2$	0	2	0	0	1	1	1	1
30	$CH_2-(OH)-CH_2$	0	1	0	0	0	0	0	0
31	CH_3-CH_2-OH	1	2	1	0	5	3	6	3
32	$CH_3-CH_2-(OH_2)$	0	2	1	4	3	1	1	2
33	CH_2-CH_2-OH	0	0	0	0	0	1	0	0
34	$CH_2-CH_2-CH_2-OH$	0	0	0	1	0	0	0	0
35	$CH_3-CH_2-CH_2-(OH_2)$	0	0	0	1	0	0	0	0
36	CH_3-O-CH_2-OH	0	0	0	1	1	1	0	0
37	$CH_3-O-CH-(OH_2)$	0	0	0	0	0	0	1	0
38	$(H_2O)-CH_2-OH$	2	1	1	0	1	2	2	1
39	$(H_2O)-CH_2-(OH_2)$	0	1	1	0	0	2	0	1
40	$(H_2O)-CH-(OH_2)$	0	0	1	0	0	0	0	0
41	$(H_2O)-CH_2-O-CH_3$	0	0	1	0	0	0	0	0
42	$CH_2-O-CH=CH_2$	0	1	0	0	0	0	0	0
43	$O=C-CH=OH$	0	1	0	0	0	0	0	0
44	$CH_3-CH=OH$	0	1	0	1	2	0	0	1
45	$CH_2=C-OH$	2	0	1	1	1	1	1	1
46	$CH_2=C-(OH_2)$	0	0	0	1	0	0	0	0
47	$CH=CH-(OH_2)$	0	0	1	0	0	0	0	0
48	$CH\equiv C-OH$	0	0	3	0	1	0	1	1
49	$CH_2=CH-OH$	0	1	1	0	0	0	0	0
50	$C\equiv CH-OH$	0	0	0	0	0	1	0	0
51	$CH_2=C=O$	0	0	0	1	1	0	1	0
52	$HO-C\equiv C-OH$	0	0	1	0	0	0	0	0
53	$CH_3-C=O$	0	0	2	0	0	0	0	0
54	CH_3-CO-H	0	1	0	0	2	0	0	0
total		196	215	230	167	257	161	138	195

Table 6. Summary of the Number of Volatiles Molecules, H and OH Radicals Formed in Each Proton Bombardment Simulation Run of the CH_4:H_2O (1:1) Ice, Along with the Averages

formula	run 1	run 2	run 3	run 4	run 5	run 6	run 7	ave
H	403	465	498	426	481	374	314	423
H_2	508	574	596	511	713	469	313	526
OH	6	6	4	9	7	7	11	7
O_2	1	1	0	0	0	0	0	0
CO	2	5	3	5	3	2	1	3
CO_2	1	1	0	0	1	0	0	0

(structure 42), hydroxyethynyl radical (structure 50), and acetyl (structure 53).

We also produced several hydrocarbon radicals stabilized by forming complexes with water molecules. For the case of $C_xH_y(H_2O)_n$, the most abundant were methyl radicals complexed with water molecule(s) via either the oxygen atom (structure 11) or the hydrogen atom(s) (structures 12 and 13). We also obtained a few methylene water complexes (structure 39), a methylidyne water complex (structure 40), a few ethyl water complexes (structure 32), a propyl water complex (structure 35), a vinylidene water complex (structure 46), and an ethenediide water complex (structure 47). For the case of $C_xH_yO_z(H_2O)_n$, the hydroxymethyl water complex (structure 38) was the dominant species formed with minor species, such as methoxy carbene (structure 37) and methoxymethyl (structure 41).

CO, CO_2, and H_2CO have been obtained in previous laboratory experiments (e.g., Moore and Hudson,[33] and Palumbo[62]). Several intermediates and products formed in our simulations could potentially form H_2CO with more impacts. The formation of CO and CO_2 requires total loss of H from carbon and oxygen; given the doses and time scales in our simulations, we do not expect them to be produced.

Figure 6 shows that in our simulations, 80% of the species formed are oxygenated and 20% are nonoxygenated. Almost all the oxygenated species are water−radical complexes (93.7%), and the remaining species are ethers (3.7%), alcohols (2.1%), and ketones (0.5%). Nonoxygenated species are mostly alkanes (70.8%; −2.9% with respect to pure methane), followed by alkenes (25%; + 1.3% with respect to pure methane) and alkynes (4.2%; + 1.6% with respect to pure methane).

https://doi.org/10.1021/acsearthspacechem.4c00225
ACS Earth Space Chem. 2024, 8, 2509−2521

3.3.2. Temporal Evolution of Molecular Formation. The temporal evolutions of the main products formed during the irradiation of CH_4 and CH_4:H_2O (1:1) ices are shown in Figure 10. We include data for ethane (structure 1), ethyl

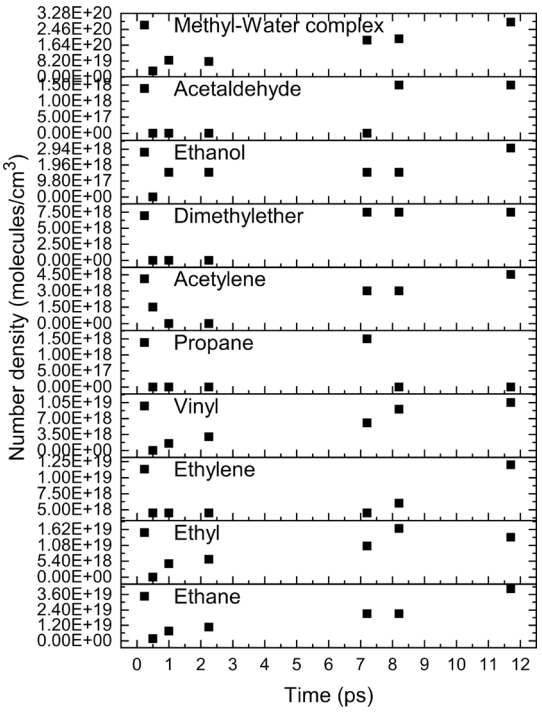

Figure 10. Number density of molecules formed as a function of time in case 2 simulation of the CH_4:H_2O 1:1 ice. The range of values for the *y*-axis varies for each molecule.

radical (structure 2), ethylene (structure 15), vinyl radical (structure 16), propane (structure 7), acetylene (structure 18), dimethyl ether (structure 24), ethanol (structure 31), acetaldehyde (structure 54), and the methyl−water complex (structure 11).

As the irradiation time increases, the number of methane−water complexes increases. The proton bombardment generates methyl radicals that are stabilized by a nearby water molecule. This considerably reduces the number of other types of molecules formed. The temporal evolution profiles for the different products show larger variations than those for CH_4. Ethane, ethyl radical, vinyl radical, and ethanol already form during the first 2 ps, with ethane being the most abundant, followed by ethyl radical, which is derived from ethane by hydrogen abstraction. Ethanol can form by the reaction of an ethyl radical with an OH radical. The presence of H_2O prevents the formation of hydrocarbons with three carbons (e.g., propane) or more. While ethylene's formation starts increasing only after 8 ps, the vinyl radical starts forming at 1 ps and the rate steadily increases with time, which suggests that the vinyl radical does not form by hydrogen abstraction from ethylene. Products that require several reaction steps to form, such as acetylene, dimethyl ether, and acetaldehyde, have temporal evolution profiles with a flat profile of zero or small production, followed by asymptotic growth. Aldehyde is the most complex molecule, and its flat profile extends the most, up to 7 ps. Despite the complexation of radicals by H_2O, a variety of molecules still form although in much smaller amounts than for CH_4. The production of organics is expected to grow as the temperature increases, which allows to overcome the reaction barriers associated with the water complexes. In terms of general trends, the population of longer-chain hydrocarbon products is smaller than that of smaller-chain hydrocarbon products. This highlights the fact that larger products take longer to form and require multiple impact, radicalization, and reaction cycles to be incrementally built up from smaller products.

3.4. Irradiation of the CH_4:H_2O (4:1) Ice. To understand the effect of the CH_4:H_2O ratio on the type and amount of products formed, we have performed a simulation using a CH_4:H_2O ratio of 4:1 for a duration of 11.6 ps and using 322 H^+ impacts (dose of 18.2 eV/molecule). The simulation led to the formation of 480 molecules. Most of the structures obtained in the simulation were also formed in the irradiation of the CH_4:H_2O (1:1) ice, and we list their molecular structures and numbers in Table 7. Four additional radical

Table 7. Summary of the Number of Molecules (See Figure 9) Formed in the Proton Bombardment Simulation Run of the CH_4:H_2O (4:1) Ice

molecule	formula	number
1	CH_3-CH_3	88
2	CH_3-CH_2	72
3	CH_3-CH	5
4	CH_3-C	1
7	$CH_3-CH_2-CH_3$	2
8	$CH_3-CH_2-CH_2$	4
11	$CH_3-(OH_2)$	218
15	$CH_2=CH_2$	25
16	$CH_2=CH$	32
17	$CH_2=C$	2
18	$CH\equiv CH$	7
21	$CH_3-C=CH_2$	1
22	$CH_3-CH=CH_2$	2
24	CH_3-O-CH_3	5
25	CH_3-O-CH_2	3
28	$CH_3-(OH)-CH_3$	2
31	CH_3-CH_2-OH	2
32	$CH_3-CH_2-(OH_2)$	3
44	$CH_3-CH=OH$	1
45	$CH_2=C-OH$	1

molecules (one for each molecule) were also formed, namely, $CH_3-CH-CH_2-CH$, CH_2-CH_2-CH, $CH_2=OH$, and $CH_3-O-CHO-CH_3$. We formed H (1504) and H_2 (1329) with OH (6) and CO (2) as minor products. O_2 and CO_2 did not form.

In Figure 7, we show the breakdown of the species produced. Increasing the number of methane molecules by a factor of 4 leads to a significant increase in the number of hydrocarbons. The ratio of oxygenated versus nonoxygenated is close to 1:1, as opposed to 80% oxygenated versus 20% nonoxygenated for the 1:1 ratio. Almost all the oxygenated species are water−radical complexes (92.4%), and the remaining species are ethers (4.2%), alcohols (2.5%), and ketones (0.8%), in agreement with the findings for the 1:1 ratio. Nonoxygenated species are mostly alkanes (71.6%; −2.1% with respect to pure methane), followed by alkenes (25.5%; +1.8% with respect to pure methane) and alkynes (2.9%; +0.3% with respect to pure methane) and comparable to the 1:1 ratio and for pure CH_4.

https://doi.org/10.1021/acsearthspacechem.4c00225
ACS Earth Space Chem. 2024, 8, 2509−2521

4. CONCLUSIONS

We have developed a new MD approach to simulate the chemistry involved in the solar wind irradiation of ices using protons with an impact velocity of 400 km/s. We have implemented an electron stopping process, in which the kinetic energy of the H^+ lost in the impact is distributed equally to neighboring molecules, and we have used a multiple impact approach, with seven protons hitting the surface, and repeated multiple times, to simulate a continuous bombardment. This approach allows for the formation of numerous complex molecules detected in previous laboratory experiments. For pure CH_4 ice, hydrocarbons form readily and in large amounts, with alkanes being predominant (73.7%), followed by alkenes (23.7%) and alkynes (2.6%). The production of ethane, ethyl radical, and ethylene grows almost monotonically, and for vinyl, propane, and acetylene, the growth accelerates at longer times (after 30 ps). The temporal evolution of propene shows that the concentration reaches a maximum at around 30 ps before decreasing to negligible concentrations at longer times, consistent with propene being an intermediate species. Interestingly, the number of methane complexes decreases over time. For CH_4:H_2O ices, the predominant species is a methyl−water complex that grows with irradiation time. Alkanes, alkenes, and alkynes form in similar proportions as for pure CH_4 although nonoxygenated molecules constitute only 20% of the products with the remaining 79.6% being oxygenated molecules. Ethers (3.7%) and alcohols (2.1%) form in comparable amounts with ketones being a very minor component (0.5%). Water inhibits the formation of hydrocarbon molecules as it solvates the methyl radicals formed. We anticipate that increasing the temperature is needed to overcome the reaction barriers due to solvation and to form organic residues.

AUTHOR INFORMATION

Corresponding Author

Alessandra Ricca − *NASA Ames Research Center, Moffett Field, California 94035-1000, United States; Carl Sagan Center, SETI Institute, Mountain View, California 94043, United States;* orcid.org/0000-0002-3141-0630; Email: alessandra.ricca-1@nasa.gov

Author

Justin B. Haskins − *Thermal Protection Materials Branch, NASA Ames Research Center, Moffett Field, California 94035, United States;* orcid.org/0000-0003-4435-9018

Complete contact information is available at: https://pubs.acs.org/10.1021/acsearthspacechem.4c00225

Notes

The authors declare no competing financial interest.

ACKNOWLEDGMENTS

A.R. and J.B.H. thank NASA's Solar System Workings (SSW; 80NSSC21K0776) program for its generous support of this work.

REFERENCES

(1) Lacy, J. H.; Carr, J. S.; Evans, I.; Neal, J.; Baas, F.; Achtermann, J. M.; Arens, J. F. Discovery of interstellar methane: Observations of gaseous and solid CH 4 absorption toward young stars in molecular clouds. *Astrophys. J.* **1991**, *376*, 556−560.

(2) Chiar, J. E.; Tielens, A. G. G. M.; Whittet, D. C. B.; Schutte, W. A.; Boogert, A. C. A.; Lutz, D.; van Dishoeck, E. F.; Bernstein, M. P. The composition and distribution of dust along the line of sight toward the Galactic Center. *Astrophys. J.* **2000**, *537*, 749−762.

(3) Chiar, J. E.; Adamson, A. J.; Pendleton, Y. J.; Whittet, D. C. B.; Caldwell, D. A.; Gibb, E. L. Hydrocarbons, ices, and "XCN" in the line of sight toward the Galactic Center. *Astrophys. J.* **2002**, *570*, 198−209.

(4) Gibb, E. L.; Whittet, D. C. B.; Boogert, A. C. A.; Tielens, A. G. G. M. Interstellar ice: The Infrared Space Observatory Legacy. *Astrophys. J., Suppl. Ser.* **2004**, *151*, 35−73.

(5) Dartois, E. The ice survey opportunity of ISO. *Space Sci. Rev.* **2005**, *119*, 293−310.

(6) Boogert, A. A.; Gerakines, P. A.; Whittet, D. C. Observations of the icy Universe. *Annu. Rev. Astron. Astrophys.* **2015**, *53*, 541−581.

(7) Boogert, A. C. A.; Schutte, W. A.; Tielens, A. G. G. M.; Whittet, D. C. B.; Helmich, F. P.; Ehrenfreund, P.; Wesselius, P. R.; de Graauw, T.; Prusti, T. Solid methane toward deeply embedded protostars. *Astron. Astrophys.* **1996**, *315*, L377−L380.

(8) Boogert, A. C. A.; Blake, G. A.; Öberg, K. Methane abundance variations toward the massive protostar NGC 7538 IRS 9. *Astrophys. J.* **2004**, *615*, 344−353.

(9) McClure, M. K.; Rocha, W.; Pontoppidan, K.; Crouzet, N.; Chu, L. E.; Dartois, E.; Lamberts, T.; Noble, J.; Pendleton, Y.; Perotti, G.; et al. An Ice Age JWST inventory of dense molecular cloud ices. *Nat. Astron.* **2023**, *7*, 431−443.

(10) Rocha, W. R. M.; van Dishoeck, E. F.; Ressler, M. E.; van Gelder, M. L.; Slavicinska, K.; Brunken, N. G. C.; Linnartz, H.; Ray, T. P.; Beuther, H.; Caratti o Garatti, A.; et al. JWST Observations of Young protoStars (JOYS+): Detecting icy complex organic molecules and ions. I. CH_4, SO_2, $HCOO^-$, OCN^-, H_2CO, HCOOH, CH_3CH_2OH, CH_3CHO, CH_3OCHO, and CH_3COOH. *Astron. Astrophys.* **2024**, *683*, A124−156.

(11) Öberg, K. I.; Boogert, A. C. A.; Pontoppidan, K. M.; Blake, G. A.; Evans, N. J.; Lahuis, F.; van Dishoeck, E. F. The c2d Spitzer spectroscopic survey of ices around Low-Mass Young Stellar Objects. III. CH_4. *Astrophys. J.* **2008**, *678*, 1032−1041.

(12) Mumma, M. J.; Charnley, S. B. The chemical composition of comets—emerging taxonomies and natal heritage. *Annu. Rev. Astron. Astrophys.* **2011**, *49*, 471−524.

(13) Gudipati, M. S.; Castillo-Rogez, J. *The science of Solar system ices*; Springer Science & Business Media: 2012; Vol. *356*.

(14) Brown, M. E. The compositions of Kuiper Belt Objects. *Annu. Rev. Earth Planet. Sci.* **2012**, *40*, 467−494.

(15) Douté, S.; Schmitt, B.; Quirico, E.; Owen, T. C.; Cruikshank, D. P.; de Bergh, C.; Geballe, T. R.; Roush, T. L. Evidence for methane segregation at the surface of Pluto. *Icarus* **1999**, *142*, 421−444.

(16) Merlin, F.; Alvarez-Candal, A.; Delsanti, A.; Fornasier, S.; Barucci, M. A.; DeMeo, F. E.; de Bergh, C.; Doressoundiram, A.; Quirico, E.; Schmitt, B. Stratification of methane ice on Eris' surface. *Astron. J.* **2009**, *137*, 315−328.

(17) Johnson, R. E. *Energetic charged-particle interactions with atmospheres and surfaces*; Springer: 1990.

(18) Mewaldt, R. A.; Cohen, C. M. S.; Mason, G. M.; Cummings, A. C.; Desai, M. I.; Leske, R. A.; Raines, J.; Stone, E. C.; Wiedenbeck, M. E.; von Rosenvinge, T. T.; et al. On the differences in composition between solar energetic particles and solar wind. *Space Sci. Rev.* **2007**, *130*, 207−219.

(19) Mewaldt, R. A.; Cohen, C. M. S.; Mason, G. M.; Haggerty, D. K.; Desai, M. I. Long-term fluences of solar energetic particles from H to Fe. *Space Sci. Rev.* **2007**, *130*, 323−328.

(20) Bennett, C. J.; Pirim, C.; Orlando, T. M. Space-weathering of solar system bodies: A laboratory perspective. *Chem. Rev.* **2013**, *113*, 9086−9150.

(21) Rothard, H.; Domaracka, A.; Boduch, P.; Palumbo, M. E.; Strazzulla, G.; Da Silveira, E. F.; Dartois, E. Modification of ices by cosmic rays and solar wind. *J. Phys. B: At., Mol. Opt. Phys.* **2017**, *50*, No. 062001.

(22) Herbst, E.; van Dishoeck, E. F. Complex organic interstellar molecules. *Annu. Rev. Astron. Astrophys.* **2009**, *47*, 427−480.
(23) Emery, J.; Wong, I.; Brunetto, R.; Cook, J.; Pinilla-Alonso, N.; Stansberry, J.; Holler, B.; Grundy, W.; Protopapa, S.; Souza-Feliciano, A.; et al. A tale of 3 dwarf planets: Ices and organics on Sedna, Gonggong, and Quaoar from JWST spectroscopy. *Icarus* **2024**, *414*, No. 116017.
(24) Pinilla-Alonso, N.; Licandro, J.; Brunetto, R.; Henault, E.; Schambeau, C.; Guilbert-Lepoutre, A.; Stansberry, J.; Wong, I.; Lunine, J.; Holler, B. et al.. Unveiling the ice and gas nature of active centaur (2060) Chiron using the James Webb Space Telescope. arXiv preprint arXiv:2407.07761 2024.
(25) Strazzulla, G.; Leto, G.; Baratta, G. A.; Spinella, F. Ion irradiation experiments relevant to cometary physics. *J. Geophys. Res.: Plenets* **1991**, *96*, 17547−17552.
(26) Strazzulla, G.; Baratta, G.; Palumbo, M. Vibrational spectroscopy of ion-irradiated ices. *Spectrochim. Acta, Part A* **2001**, *57*, 825−842.
(27) Ferini, G.; Baratta, G. A.; Palumbo, M. E. A Raman study of ion irradiated icy mixtures. *Astron. Astrophys.* **2004**, *414*, 757−766.
(28) Palumbo, M. E.; Ferini, G.; Baratta, G. A. Infrared and Raman spectroscopies of refractory residues left over after ion irradiation of nitrogen-bearing icy mixtures. *Adv. Space Res.* **2004**, *33*, 49−56.
(29) Kaiser, R. I.; Roessler, K. Theoretical and laboratory studies on the interaction of cosmic-ray particles with interstellar ices. III. Suprathermal chemistry-induced formation of hydrocarbon molecules in solid methane (CH_4), ethylene (C_2H_4), and acetylene (C_2H_2). *Astrophys. J.* **1998**, *503*, 959−975.
(30) Bennett, C. J.; Jamieson, C. S.; Osamura, Y.; Kaiser, R. I. Laboratory studies on the irradiation of methane in interstellar, cometary, and Solar System ices. *Astrophys. J.* **2006**, *653*, 792−811.
(31) Jones, B. M.; Kaiser, R. I. Application of reflectron time-of-flight mass spectroscopy in the analysis of astrophysically relevant ices exposed to ionization radiation: Methane (CH4) and D4-methane (CD4) as a case study. *J. Phys. Chem. Lett.* **2013**, *4*, 1965−1971.
(32) Abplanalp, M. J.; Jones, B. M.; Kaiser, R. I. Untangling the methane chemistry in interstellar and solar system ices toward ionizing radiation: a combined infrared and reflectron time-of-flight analysis. *Phys. Chem. Chem. Phys.* **2018**, *20*, 5435−5468.
(33) Moore, M.; Hudson, R. Infrared study of ion-irradiated water-ice mixtures with hydrocarbons relevant to comets. *Icarus* **1998**, *135*, 518−527.
(34) Mifsud, D. V.; Herczku, P.; Sulik, B.; Juhász, Z.; Vajda, I.; Rajta, I.; Ioppolo, S.; Mason, N. J.; Strazzulla, G.; Kaňuchová, Z. Proton and electron irradiations of CH4:H2O mixed ices. *Atoms* **2023**, *11*, 19.
(35) Bergantini, A.; Maksyutenko, P.; Kaiser, R. I. On the formation of the C_2H_6O isomers ethanol (C_2H_5OH) and dimethyl ether (CH_3OCH_3) in star-forming regions. *Astrophys. J.* **2017**, *841*, 96−120.
(36) Turner, A. M.; Kaiser, R. I. Exploiting photoionization reflectron time-of-flight mass spectrometry to explore molecular mass growth processes to complex organic molecules in interstellar and Solar System ice analogs. *Acc. Chem. Res.* **2020**, *53*, 2791−2805.
(37) Shingledecker, C. N.; Herbst, E. A general method for the inclusion of radiation chemistry in astrochemical models. *Phys. Chem. Chem. Phys.* **2018**, *20*, 5359−5367.
(38) Shingledecker, C. N.; Vasyunin, A.; Herbst, E.; Caselli, P. On simulating the proton-irradiation of O2 and H2O ices using astrochemical-type models, with implications for bulk reactivity. *Astrophys. J.* **2019**, *876*, 140−150.
(39) Pilling, S.; Carvalho, G. A.; Rocha, W. R. M. Chemical evolution of CO2 ices under processing by ionizing radiation: Characterization of nonobserved species and chemical equilibrium phase with the employment of PROCODA code. *Astrophys. J.* **2022**, *925*, 147−177.
(40) Shingledecker, C. N.; Incerti, S.; Ivlev, A.; Emfietzoglou, D.; Kyriakou, I.; Vasyunin, A.; Caselli, P. Cosmic-ray tracks in astrophysical ices: Modeling with the Geant4-DNA Monte Carlo Toolkit. *Astrophys. J.* **2020**, *904*, 189−202.
(41) van Duin, A. C. T.; Dasgupta, S.; Lorant, F.; Goddard, W. A. ReaxFF: A reactive force field for hydrocarbons. *J. Phys. Chem. A* **2001**, *105*, 9396−9409.
(42) Anders, C.; Urbassek, H. M. Solar wind ion impacts into ice surfaces: A molecular-dynamics study using the REAX force field. *Icarus* **2017**, *282*, 351−362.
(43) Boduch, P.; Dartois, E.; de Barros, A. L.; da Silveira, E. F.; Domaracka, A.; Lv, X.-Y.; Palumbo, M. E.; Pilling, S.; Rothard, H.; Duarte, E. S.; et al. Radiation effects in astrophysical ices. *J. Phys: Conf. Ser.* **2015**, *629*, No. 012008.
(44) Dartois, E.; Augé, B.; Boduch, P.; Brunetto, R.; Chabot, M.; Domaracka, A.; Ding, J. J.; Kamalou, O.; Lv, X. Y.; Rothard, H.; et al. Heavy ion irradiation of crystalline water ice. Cosmic ray amorphisation cross-section and sputtering yield. *Astron. Astrophys.* **2015**, *576*, A125.
(45) Martínez, L.; Andrade, R.; Birgin, E. G.; Martínez, J. M. PACKMOL: A package for building initial configurations for molecular dynamics simulations. *J. Comput. Chem.* **2009**, *30*, 2157−2164.
(46) Chenoweth, K.; van Duin, A. C. T.; Goddard, W. A. ReaxFF Reactive Force Field for molecular dynamics simulations of hydrocarbon oxidation. *J. Phys. Chem. A* **2008**, *112*, 1040−1053.
(47) Ziegler, J. F. SRIM-2003. *Nucl. Instrum. Methods Phys. Res. B: Beam Interact. Mater. At.* **2004**, *219*−*220*, 1027−1036.
(48) Thompson, A. P.; Aktulga, H. M.; Berger, R.; Bolintineanu, D. S.; Brown, W. M.; Crozier, P. S.; in't Veld, P. J.; Kohlmeyer, A.; Moore, S. G.; Nguyen, T. D.; et al. LAMMPS - a flexible simulation tool for particle-based materials modeling at the atomic, meso, and continuum scales. *Comput. Phys. Commun.* **2022**, *271*, No. 108171.
(49) Zhang, W.; van Duin, A. C. T. Improvement of the ReaxFF description for functionalized hydrocarbon/water weak interactions in the condensed phase. *J. Phys. Chem. B* **2018**, *122*, 4083−4092.
(50) Ziegler, J. F.; Biersack, J. P. In *Treatise on Heavy-Ion Science: Vol. 6: Astrophysics, Chemistry, and Condensed Matter*; Bromley, D. A., Ed.; Springer US: Boston, MA, 1985; pp 93−129.
(51) Anders, C.; Urbassek, H. M. Impacts into cosmic ice surfaces: A molecular-dynamics study using the Reax force field. *Nucl. Instrum. Methods Phys. Res. B: Beam Interact. Mater. At.* **2013**, *303*, 200−204.
(52) Cruikshank, D.; Roush, T.; Bartholomew, M.; Geballe, T.; Pendleton, Y.; White, S.; Bell, J.; Davies, J.; Owen, T.; de Bergh, C.; et al. The composition of Centaur 5145 Pholus. *Icarus* **1998**, *135*, 389−407.
(53) Poulet, F.; Cuzzi, J.; Cruikshank, D.; Roush, T.; Dalle Ore, C. Comparison between the Shkuratov and Hapke scattering theories for solid planetary surfaces: Application to the Surface Composition of Two Centaurs. *Icarus* **2002**, *160*, 313−324.
(54) Baratta, G. A.; Leto, G.; Palumbo, M. E. A comparison of ion irradiation and UV photolysis of CH4 and CH3OH. *Astron. Astrophys.* **2002**, *384*, 343−349.
(55) Baratta, G.; Domingo, M.; Ferini, G.; Leto, G.; Palumbo, M.; Satorre, M.; Strazzulla, G. Ion irradiation of CH4-containing icy mixtures. *Nucl. Instrum. Methods Phys. Res. B: Beam Interact. Mater. At.* **2003**, *209*, 283−287.
(56) Ausloos, P.; Rebbert, R. E.; Lias, S. Direct and inert-gas-sensitized radiolysis and photolysis of methane in the solid phase. *J. Chem. Phys.* **1965**, *42*, 540−548.
(57) Gerakines, P. A.; Schutte, W. A.; Ehrenfreund, P. Ultraviolet processing of interstellar ice analogs. I. Pure ices. *Astron. Astrophys.* **1996**, *312*, 289−305.
(58) Garozzo, M.; La Rosa, L.; Kanuchova, Z.; Ioppolo, S.; Baratta, G.; Palumbo, M.; Strazzulla, G. The influence of temperature on the synthesis of molecules on icy grain mantles in dense molecular clouds. *Astronomy & Astrophysics* **2011**, *528*, A118.
(59) Abplanalp, M. J.; Förstel, M.; Kaiser, R. I. Exploiting single photon vacuum ultraviolet photoionization to unravel the synthesis of complex organic molecules in interstellar ices. *Chem. Phys. Lett.* **2016**, *644*, 79−98.
(60) Abplanalp, M. J.; Gozem, S.; Krylov, A. I.; Shingledecker, C. N.; Herbst, E.; Kaiser, R. I. A study of interstellar aldehydes and enols as

tracers of a cosmic ray-driven nonequilibrium synthesis of complex organic molecules. *Proc. Natl. Acad. Sci. U. S. A.* **2016**, *113*, 7727−7732.
(61) Zhu, C.; Wang, H.; Medvedkov, I.; Marks, J.; Xu, M.; Yang, J.; Yang, T.; Pan, Y.; Kaiser, R. I. Exploitation of synchrotron radiation photoionization mass spectrometry in the analysis of complex organics in interstellar model ices. *J. Phys. Chem. Lett.* **2022**, *13*, 6875−6882.
(62) Palumbo, M. E. Production of CO and CO_2 after ion irradiation of ices. *Adv. Space Res.* **1997**, *20*, 1637−1645.

https://doi.org/10.1021/acsearthspacechem.4c00225
ACS Earth Space Chem. 2024, 8, 2509−2521